Wu et al. *Zool. Res.* 2026, 47(2): 333−346
https://doi.org/10.24272/j.issn.2095-8137.2025.087
https://cstr.cn/32248.14.zr.2025.087

ZR | Zoological Research

Article Open Access

Distinct lateral hypothalamus GABAergic projections regulate sensory and affective dimensions of pain

Zhi-Xin Wu[1,2,3,#], Jian-Shuai Zhao[1,2,3,#], Chang Bao[1,2,3], Jian-Nan Li[1,2,3], Ting-Ting Gu[1,2,3], Hui-Min Wu[1,2,3], Bing-Qing Li[1,2,3], Meng-Ke Guo[1,2,3], Hai-Long Dong[1,2,3], Hui-Ming Li[1,2,3,*], Dan Wang[1,2,3,*]

[1] *Department of Anesthesiology and Perioperative Medicine*, *Xijing Hospital*, *Fourth Military Medical University*, *Xi'an*, *Shaanxi* 710032, *China*

[2] *Key Laboratory of Anesthesiology (Fourth Military Medical University)*, *Ministry of Education of China*, *Xi'an*, *Shaanxi* 710032, *China*

[3] *Shaanxi Provincial Clinical Research Center for Anesthesiology Medicine*, *Xi'an*, *Shaanxi* 710032, *China*

ABSTRACT

Pain encompasses both sensory discrimination and affective evaluation, yet the precise behavioral and neurobiological mechanisms of this well-conserved phenomenon are still incompletely understood. Although the lateral hypothalamus area (LHA) has been implicated in nociceptive modulation, its underlying circuitry and causal mechanisms remain elusive. In this study, formalin-induced pain-like behaviors in mice were associated with attenuated activity in LHA^{GAD2}-positive neurons, a pattern also observed during acute restraint stress in adult male transgenetic mice. Chemogenetic activation of LHA^{GAD2} neurons significantly alleviated formalin-evoked nociceptive responses and reduced aversive behavioral phenotypes. Additionally, functional analyses revealed a GABAergic projection from the LHA to the lateral habenula that selectively mitigated affective disturbances in a neuropathic pain model. In parallel, projections from LHA^{GAD2} neurons to specific neuronal subsets within the ventrolateral periaqueductal gray modulated nociceptive responses under neuropathic pain conditions. These findings delineate a dual-pathway mechanism by which LHA^{GAD2} neurons independently regulate sensory and affective dimensions of pain-like behavior, offering a basis for targeted pain relief. Collectively, the results reveal previously uncharacterized aspects of pain processing by discrete LHA GABAergic subpopulations and potentially inform the development of subregion- or cell type-specific therapies for pain management.

Keywords: Lateral hypothalamus; GABAergic neurons; Pain modulation; Neural circuits; Viral genetics

INTRODUCTION

Pain represents an evolutionarily conserved, complex phenomenon comprising distinct sensory-discriminative and affective-emotional dimensions (Bushnell et al., 2013; Gan et al., 2022). The affective response to noxious stimuli engages neural substrates that are functionally and anatomically dissociable from those encoding stimulus location, intensity, or duration (Baliki & Apkarian, 2015; Corder et al., 2019; Wu et al., 2017). Nociceptive signaling triggered by tissue damage initiates both reflexive and adaptive behavioral responses to prevent further injury (Baliki & Apkarian, 2015; Price, 2000). These processes depend on integrated neural circuits that orchestrate complex motor execution, such as immediate withdrawal from painful stimuli, threat prediction, and experience-dependent avoidance strategies (Navratilova & Porreca, 2014; Price, 2000). Although considerable advances have been made in delineating nociceptive pathways, the circuit-level mechanisms underlying various aspects of pain perception remain incompletely defined. Given the intrinsic affective nature of pain, structures implicated in emotional regulation are now recognized as central modulators of pain processing within the brain (Gan et al., 2022).

Emerging evidence highlights the crucial role of the lateral hypothalamus area (LHA) as a key integrative node in pain modulation, receiving diverse sensory inputs from the cerebral cortex and participating in the regulation of sleep-wake cycles, affective states, autonomic function, nociception, and energy homeostasis (Gan et al., 2022; Tang et al., 2022). In addition to direct neural influences, the LHA modulates pain indirectly through control of the hypothalamic-pituitary-adrenal axis, promoting glucocorticoid release with downstream anti-inflammatory effects that may alter pain sensitivity and associated comorbidities (Dhaka et al., 2007; Reddy et al.,

Received: 17 May 2025; Accepted: 10 September 2025; Online: 11 September 2025

Foundation items: This work was supported by the National Natural Science Foundation of China (82471225, 82101343 to D.W.; 82030038, 82221001 to H.L.D.)

[#]Authors contributed equally to this work

*Corresponding authors, E-mail: huimingli1218@163.com; danwang0319@126.com

2025; Shah et al., 2025; Siemian et al., 2021). Recent pharmacological studies have linked multiple neuromodulators and receptors, such as α1- and α2-adrenoceptors, cannabinoid 1 receptors, hypocretin 2 receptors, tachykinin 1 receptors, and substance P, to LHA-mediated nociceptive regulation via projections to the periaqueductal gray (PAG) (Esmaeili et al., 2017; Holden et al., 2009). However, the specific cellular substrates within the LHA that mediate pain-related functions have only recently become accessible through high-resolution genetic and neurophysiological approaches (Shah et al., 2025). Changes in emotional states, such as stress and anxiety, can affect pain perception and processing (Gan et al., 2022). Our previous work exploring the relationship between LHA and anesthesia identified functional GABAergic synaptic connections between the LHA and brain regions such as the ventrolateral PAG (vlPAG) and dorsolateral septum (Wang et al., 2024), circuits implicated in arousal, stress, and affective processing. Other LHA outputs target regions including the ventral tegmental area (VTA), central amygdala, and lateral habenula (LHb), suggesting a role of GABAergic LHA (LHA^{GABA}) neurons in emotional regulation and aversion states (He et al., 2023; Li et al., 2024; Stuber & Wise, 2016). Notably, LHA neurons receive convergent inputs from thalamic and somatosensory nociceptive pathways, as well as projections from limbic structures engaged in fear and anxiety (He et al., 2023; Zhu et al., 2017), suggesting a central role in integrating sensory inputs and affective components of pain.

This study aimed to characterize the role of LHA^{GAD2} neurons in sensory and affective pain processing by identifying their circuit mechanisms and functionally distinct subpopulations. Specifically, their involvement in pain-induced hypersensitivity and aversion behaviors was examined, and the impact of targeted manipulations on nociceptive responses was evaluated. Anatomical tracing, optogenetic and chemogenetic interventions, and *in vitro* electrophysiology were employed to delineate the circuit architecture and identify functionally distinct subsets of LHA^{GAD2} neurons. Together, these approaches defined parallel inhibitory pathways through which LHA^{GAD2} neurons selectively modulate sensory and affective components of pain-related behavior.

MATERIALS AND METHODS

Mice

All experimental protocols were approved by the Animal Experiment Ethics Committee (No. IACUC-20210651) and conducted in accordance with the Guidelines for Animal Experiments of the Fourth Military Medical University (Xi'an, China) and the ARRIVE (Animal Research: Reporting of *In Vivo* Experiments) guidelines. Adult male C57BL/6J mice and male transgenic mice (8–12 weeks old, 22–25 g) were used in all experiments, except for whole-cell patch-clamp recordings, which used mice older than 3 weeks. The C57BL/6J mice were obtained from Beijing Vital River Laboratory Animal Technology Co., Ltd., China. Vglut2-IRES-Cre and GAD2-IRES-Cre mice were originally sourced from the Jackson Laboratory (USA). Mice were housed under specific-pathogen-free conditions with a light-controlled schedule (lights on from 07:00h to 19:00h) at ambient temperature (22–24°C), controlled humidity (38%–42%), and *ad libitum* access to food and water.

Stereotaxic surgery

Surgical procedures were performed under aseptic conditions, with body temperature maintained using a heating pad. Mice were anesthetized with 1.4 vol% isoflurane (Baxter Healthcare, USA) in oxygen and positioned on a stereotaxic frame (RWD, China), with anesthesia maintained at approximately 1.0% via a face mask. Erythromycin eye ointment was applied to protect the eyes. For adeno-associated virus (AAV) microinjections, 200 nL of AAV was bilaterally injected into the LHA (AP: –1.75 mm, ML: ±0.90 mm, DV: –5.10 mm) of GAD2-Cre mice. The injection cannula was left in place for at least 10 min prior to slow withdrawal. For optogenetic fiber implantation, optical fibers (NA=0.37, 2.5 mm diameter, 200 μm fiber optical cable) were implanted above the LHA, vlPAG (AP: –4.40 mm, ML: ±0.40 mm, DV: –2.10 mm), or LHb (AP: –1.70 mm, ML: ±0.45 mm, DV: –2.70 mm). The fibers were secured to the skull with a thin layer of superglue (LOCTITE, China) and dental cement.

Optogenetic protocols

Three weeks post-injection of rAAV-Ef1α-DIO-ChR2-mCherry, rAAV-Ef1α-DIO-NpHR3.0-mCherry, or rAAV-Ef1α-DIO-mCherry into the LHA of GAD2-IRES-Cre mice, optogenetic stimulation experiments were conducted. Optical activation was performed using a 473 nm blue laser at 20 Hz, while inhibition was induced using a 580 nm yellow laser at 1 Hz (Thinker Tech, China). Stimulation frequencies were determined based on optimal parameters identified via *in vitro* electrophysiology. Laser intensity was measured using an optical power meter (SANWA Electric Instrument Co., Japan), and an unused fiber was attached to calibrate intensity to 10 mW. Implanted fibers were connected to patch cords and laser sources through rotary joints mounted over the behavioral testing apparatus.

Chemogenetic protocols (DREADDs)

To chemically manipulate LHA GABAergic neuron activity, GAD2-IRES-Cre mice in the activation group were bilaterally injected with rAAV-Ef1α-DIO-hM3D(Gq)-mCherry, while mice in the inhibition group were injected with rAAV-Ef1α-DIO-hM4D(Gi)-mCherry. Control mice were injected with rAAV-Ef1α-DIO-mCherry-WPREs. At 30 min before behavioral testing, mice were administered clozapine N-oxide (CNO, Sigma, USA) at 3 mg/kg intraperitoneally, or equivalent volumes were microinjected into the vlPAG or LHb via previously implanted guide cannulae. Control animals received equivalent volumes of saline.

Formalin-induced pain model

Mechanical hypersensitivity was induced using subcutaneous formalin injection, following previously described protocols (Mindaye et al., 2024). A 5% formalin solution was prepared in phosphate-buffered saline (PBS) at pH 7.4. After habituation to the testing environment, 10 μL of formalin was slowly injected into the plantar surface of one hind paw using a Hamilton syringe equipped with a 30G needle.

Von Frey test

Mechanical sensitivity was assessed using calibrated Von Frey filaments (North Coast Medical, USA). Mice were placed on an elevated behavioral testing platform with a 5-mm wire mesh floor and allowed to habituate for 30 min before formal testing. Filaments were applied to the plantar surface of the hind paw at 5 s intervals, with force incrementally increased

from 0.008 g to 2 g, as described previously (Zhang et al., 2021). The applied force was considered effective when the filament bent into an S-shape. Each stimulation lasted no longer than 3 s. Behavioral responses such as paw withdrawal, licking, or rapid foot reflexes were recorded as positive responses (denoted as “X”), while the absence of such responses was recorded as negative (denoted as “O”). If no withdrawal was observed, the next higher force was applied. The 50% paw withdrawal threshold was determined using the up-down method.

Thermal hyperalgesia test

Thermal hypersensitivity was evaluated by measuring paw withdrawal latency in response to radiant heat, as an index of thermal hyperalgesia (Zhang et al., 2021). Mice were habituated in individual transparent enclosures on a glass surface for 30 min before testing. A thermal stimulus was applied to the center of the hind paw using an analgesia meter (Model 336 TG, IITC Life Science, USA), and the latency to paw withdrawal was recorded. The stimulus was terminated immediately upon paw movement or after a maximum of 20 s to prevent tissue damage. The thermal stimulus intensity was consistent throughout the experiment. Each paw was subjected to three trials, with inter-trial intervals of 5–6 min, from which average latency was calculated.

To further assess radiant heat sensitivity, an additional thermal test was performed according to the Hargreaves method (Hargreaves et al., 1988). Mice were placed in a transparent Plexiglas box on a glass floor illuminated from below by a focused light beam (IITC Life Science Inc., USA) The light intensity was adjusted to yield a baseline paw withdrawal thermal latency (PWTL) of approximately 10 s. A cutoff time of 20 s was used to avoid tissue damage. Four trials per mouse were conducted at 5 min intervals, and the average latency was calculated.

Chronic constriction injury (CCI) model

Neuropathic pain was induced using a modified CCI protocol (Zhang et al., 2021). Briefly, 3-week-old mice were anesthetized with 1.4% isoflurane in oxygen, and an incision was made in the skin and underlying muscle to expose the sciatic nerve at the mid-thigh level. The nerve was loosely ligated at three sites (1 mm apart) using 5-0 non-absorbent sutures (5.0), with the first ligature positioned proximal to the trifurcation. Care was taken to minimize disruption of surrounding structures, and ligature tightness was judged sufficient when slight hind limb tremors were observed. Model success was confirmed by observation of paw licking or flipping behaviors post-surgery. Mice exhibiting overt motor deficits in the ipsilateral hind limb were excluded from further analysis to maintain the integrity of the experimental cohort.

Acute restraint stress (ARS) model

Acute stress was induced by restraining mice in 50 mL conical tubes for 2 h. Tubes were perforated to ensure adequate ventilation. Control mice were placed in standard cages without access to food or water during the restraint period but were allowed free movement.

Open field test (OFT)

Exploratory activity and anxiety-like behavior were measured using the OFT. Following a 1 h acclimation period in the testing room, each mouse was placed in the center of the open-field apparatus (40 cm×40 cm) and observed for 15 min. The arena was divided into central and peripheral zones for analysis. The trajectory of each mouse was recorded using a camera placed above the test chamber. Total distance traveled and time spent in the center zone were quantified using ANY-maze software, as described previously (Wang et al., 2021). The apparatus was cleaned with 75% ethanol after each session.

Elevated plus maze (EPM) test

Anxiety-like behavior was further evaluated using an EPM consisting of two open arms and two closed arms (each 40 cm long, 10 cm wide) elevated 50 cm above the floor. The closed arms were enclosed by a 20 cm-high black wall. Each mouse was placed on the central platform facing an open arm and allowed to explore the maze for 5 min. Time spent in the open and closed arms was recorded (Wang et al., 2021). The platform was cleaned with 75% ethanol and air-dried for 5 min between trials.

Real-time place aversion (RTPA) test

Place preference or aversion was measured using a specially designed two-chamber apparatus composed of a white light box and a black dark box (30 cm long×30 cm wide×30 cm high). During the adaptive phase, mice were placed in the center of the apparatus and allowed to explore both chambers for 5 min without light stimulation. During the stimulation phase, mice were allowed to move freely between the light and dark chambers; optical stimulation (473 nm blue or 580 nm yellow light) was applied only when the head entered or remained in the dark box. Stimulation ceased upon exit. Mice were allowed to explore the area for 5 min, and total distance traveled and time spent in each compartment were recorded.

Immunofluorescence staining

Mice were euthanized by intraperitoneal injection of 10% potassium chloride (KCl) and perfused transcardially with 10 mL of 0.9% saline followed by 10 mL of 4% paraformaldehyde. Brains were coronally sliced at 40 μm thickness using a freezing microtome (Leica CM1900, Germany). Slices were rinsed in PBS, blocked for 2 h at room temperature in 5% standard donkey serum with 0.3% Triton X-100, and incubated for at least 24 h at 4°C with primary antibodies: anti-c-Fos (226008, Synaptic Systems; 1:1 000, Germany) and anti-GAD65 (MAB351, Sigma-Aldrich; 1:200, USA). After washing with PBS, sections were incubated for 2 h at room temperature with secondary antibodies: donkey anti-rabbit IgG Alexa Fluor 594 (711-545-152, Jackson ImmunoResearch; 1:500, USA) and donkey anti-mouse IgG Alexa Fluor 488 (715-545-150, Jackson ImmunoResearch; 1:500, USA). Brain slices were mounted and imaged using a laser confocal fluorescence microscope. Neuron counts were performed using ImageJ software.

Monosynaptic rabies virus (RV) retrograde tracing

To map upstream neurons projecting to the LHA and LHA GABAergic pathways, Cre-dependent monosynaptic RV tracing was conducted. Mice were anesthetized with sodium pentobarbital (40 mg/kg) and secured in a stereotaxic frame (RWD Life Science, China). Viruses were injected according to the stereotaxic coordinates using a pulled glass micropipette attached to a syringe pump at a rate of 50 nL/min. AAV-DIO-TVA-GFP and AAV-DIO-RVG viral solutions (200 nL) were unilaterally microinjected into the LHb of Vglut2-Cre mice and the LHA or vlPAG of GAD2-Cre mice. After a 3-week expression period, 200 nL of RV-EnvA-ΔG-dsRed (RV) was unilaterally injected into the LHb of Vglut2-

Cre mice or the LHA, LHb or vlPAG of GAD2-Cre mice. Following a 10-min diffusion period, the micropipette was slowly retracted. Tissue samples were collected 1 week after RV microinjection.

***In vitro* electrophysiology and whole-cell recordings**

Acute coronal brain slices containing the LHA (300 μm thick) were generated using a vibratome (VT1200S, Leica, Germany) in ice-cold N-methyl-D-glucamine (NMDG) cutting solution (in mmol/L): 92 NMDG, 2.5 KCl, 1.25 NaH_2PO_4, 30 $NaHCO_3$, 20 HEPES, 25 glucose, 2 thiourea, 5 Na-ascorbate, 3 Na-pyruvate, 0.5 $CaCl_2$, and 10 $MgSO_4$ (oxygenated with 95% O_2 and 5% CO_2). Slices were incubated in recording artificial cerebrospinal fluid (ACSF) (in mmol/L): 124 NaCl, 2.5 KCl, 1.25 NaH_2PO_4, 24 $NaHCO_3$, 12.5 glucose, 5 HEPES, 2 $CaCl_2$, and 2 $MgSO_4$ for 45 min at 35°C, followed by 1 h at room temperature (22–26°C) before transfer to the recording chamber (Li et al., 2025).

Recording micropipettes (4–6 MΩ) were pulled from borosilicate glass capillaries (1.5 mm OD, 0.86 mm ID) using a horizontal puller (P-97, Sutter Instruments). The Cs^+ pipette solution for optically induced inhibitory postsynaptic current (oIPSC) recordings contained (in mmol/L): 120 cesium methane sulfonate, 10 HEPES, 10 sodium phosphocreatine, 8 NaCl, 1 QX-314, 0.5 EGTA, 4 Mg-ATP, and 0.4 Na_2-GTP. Whole-cell recordings were acquired using an Axon 700B amplifier, with continuous ACSF perfusion (3–5 mL/min) at room temperature. After achieving whole-cell configuration, recordings were initiated following a 3–5 min stabilization period. For oIPSC recordings, neurons were voltage-clamped at 0 mV. Excitatory synaptic transmission was pharmacologically blocked by bath application of DL-APV (100 mmol/L) and CNQX (20 mmol/L). ChR2-expressing fibers were stimulated using 473 nm light pulses (3–5mW, duration 1–2 ms), and postsynaptic currents were recorded. Pharmacological agents including picrotoxin (100 μmol/L), TTX (0.5 μmol/L), and TTX+4AP (100 μmol/L) were bath applied as needed. Data were low-pass filtered at 2 kHz, digitized at 10 kHz, and acquired using pCLAMP v.10.6 (Molecular Devices, USA). The recorded oIPSCs were subsequently analyzed using Clampfit v10.6 (Molecular Devices, USA) (Li et al., 2025).

Statistical analysis

All analyses were conducted by investigators blinded to the experimental groups. Statistical analyses were performed using GraphPad Prism v.9.0 (GraphPad Software, USA). Parametric data are presented as mean±standard error of the mean (SEM). Group comparisons were performed using paired or unpaired two-tailed Student's *t*-tests. Behavioral data were analyzed using one-, two-, or three-way mixed model analysis of variance (ANOVA), followed by Bonferroni or Dunnett's *post hoc* tests for multiple comparisons. The chi-square test was used to assess differences in cell counts from the RV tracing experiments. Behavioral testing conditions were counterbalanced between experimental and control groups, except for optogenetic manipulations. Statistical significance was set at $P<0.05$.

RESULTS

Formalin and ARS induce maladaptive behaviors in male mice

Pain-related and anxiety-like behaviors were assessed following formalin injection and ARS exposure. In the formalin model, nociceptive sensitivity was evaluated at 0.5 h, 2 h, 24 h, and 3 days post-injection using the Von Frey and Hargreaves tests, while anxiety-like behaviors were assessed on day 3 using the OFT and EPM (Figure 1A). Formalin-treated mice exhibited a significant reduction in paw withdrawal mechanical threshold (PWMT) (Figure 1B) and PWTL (Figure 1C), indicating enhanced pain sensitivity. Behavioral assessment based on the OFT revealed reductions in total distance traveled (Figure 1E), average speed (Figure 1F), and time spent and distance traveled in the center zone (Figure 1G, H). In the EPM, formalin-injected mice displayed increased time spent in the closed arms (Figure 1J) and reduced time in the open arms (Figure 1L), indicative of elevated anxiety-like behavior.

To evaluate stress-induced behavioral alterations, anxiety-like phenotypes were assessed 4–6 h after ARS using the OFT and EPM (Figure 2A). In the OFT, ARS-exposed mice showed significant reductions in total distance traveled, average speed, and time spent and distance traveled in the center zone (Figure 2B–E). In the EPM, ARS-exposed mice spent more time in the closed arms, less time in the open arms, and exhibited increased line crossings (Figure 2G–J), consistent with anxiety-like responses.

These findings demonstrate that both formalin-induced inflammation and ARS elicit maladaptive behavioral states in mice, characterized by enhanced pain sensitivity and elevated anxiety levels.

LHA^{GAD2} neurons modulate ARS-induced anxiety and aversion

Immunofluorescence analysis revealed elevated c-Fos expression in the LHA following ARS, accompanied by a significant reduction in the proportion of c-Fos-positive neurons co-expressing GAD2 (Figure 2K; Supplementary Figure S1A, B). To investigate whether direct optogenetic activation of LHA^{GAD2} neurons reduces ARS-induced anxiety and aversive behaviors, GAD2-Cre mice received LHA-targeted injections of rAAV-EF1α-DIO-ChR2-mCherry, rAAV-DIO-NpHR3.0-mCherry, or AAV-DIO-mCherry, followed by optical fiber implantation. ARS was performed 3 weeks post-injection, and optogenetic stimulation was delivered 4–6 h later to manipulate LHA^{GAD2} neuron activity. Behavioral responses were assessed using the OFT and EPM (Figure 2M). Activation of LHA^{GAD2} neurons with 473 nm light increased average speed, total distance traveled, and both time spent and distance traveled in the center zone during the OFT (Figure 2N–R). In the EPM, activation decreased time spent in the closed arms, increased time spent in the open arms, and increased line crossings (Figure 2S–W), reflecting attenuation of ARS-induced anxiety-like behavior. Conversely, inhibition of LHA^{GAD2} neurons using 580 nm light reduced average speed, total distance traveled, and time spent and distance traveled in the center zone in the OFT (Supplementary Figure S1I–L). In the EPM, inhibition elevated time spent in the closed arms, decreased time spent and distance traveled in the open arms, and decreased line crossings (Supplementary Figure S1R–U), consistent with heightened anxiety-like responses. No significant behavioral changes were observed in control animals expressing mCherry alone (Supplementary Figure S1D–H, M–Q).

A two-chamber RTPA paradigm was employed to evaluate affective responses to LHA^{GAD2} modulation (Figure 3A).

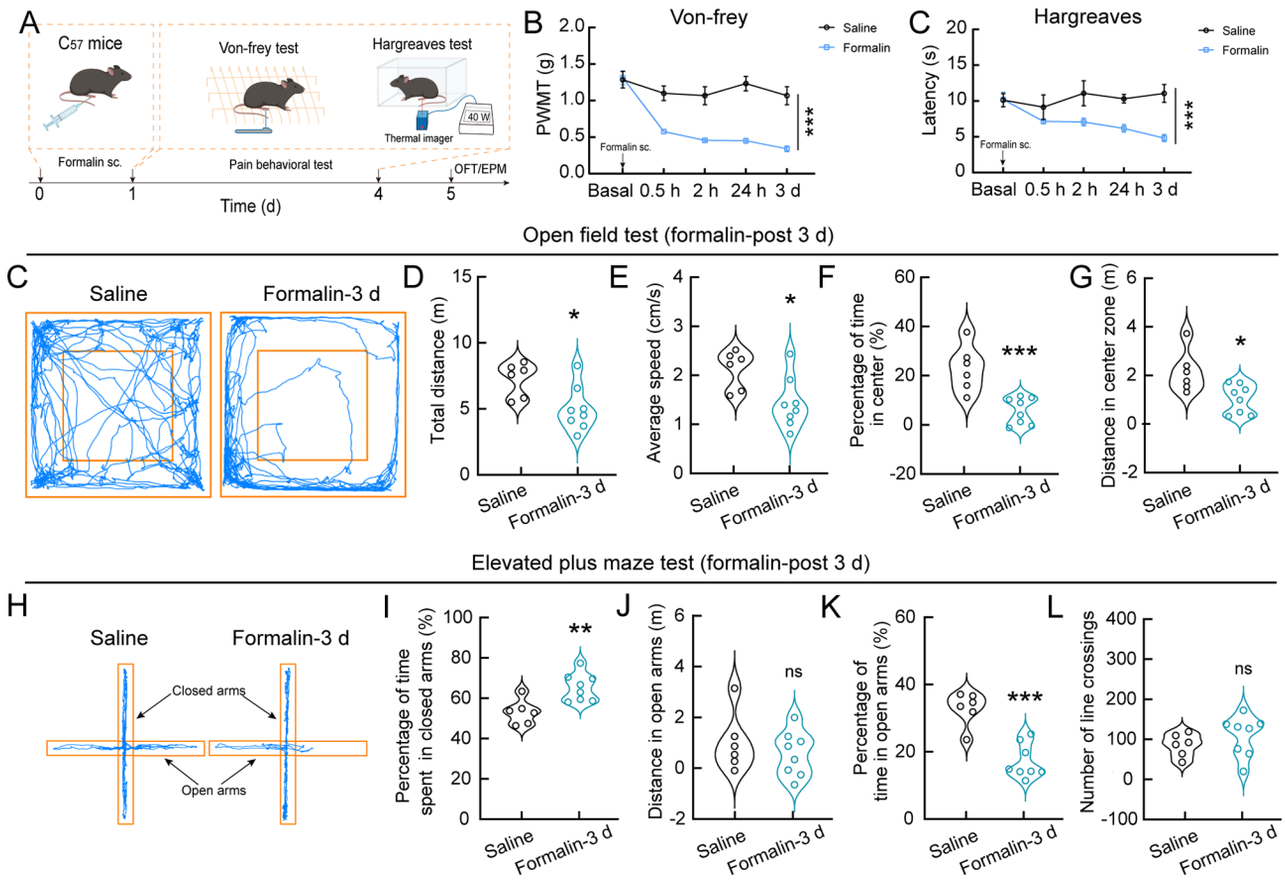

Figure 1 Subcutaneous formalin injection induces pain- and anxiety-like behaviors in mice

A: Schematic of experimental design for behavioral testing following induction of the pain model. B, C: Paw withdrawal mechanical threshold (PWMT) and paw withdrawal thermal latency (PWTL) after subcutaneous injection of formalin or saline in mice. Repeated-measures (RM) two-way ANOVA with Tukey's *post hoc* test, ***: P<0.001, n=6 in saline group, n=8 in formalin group. C–G: Open field test comparing movement trajectory (C), total distance traveled (D), average speed (E), percentage of time spent in center zone (F), and distance traveled in center zone (G) between formalin and saline groups. H–L: Elevated plus maze test comparing movement trajectory (H), percentage of time spent in closed arms (I), distance traveled in open arms (J), percentage of time spent in open arms (K), and number of lines crossing (L) between formalin and saline groups. Data analyzed using two-tailed unpaired *t*-test. ns: Not significant; *: $P<0.05$; **: $P<0.01$; ***: $P<0.001$. n=6 in saline group, n=8 in formalin-3d group. Data are presented as mean±SEM.

Optogenetic activation or inhibition of LHA^{GAD2} neurons was applied when the test mouse head entered or remained in the dark box. During the conditioning test phase, mice in the NpHR group spent significantly less time in the dark chamber than those in the mCherry control group (Figure 3B, right, C, D). Mice spent more time in the conditioned chamber during 473 nm laser stimulation (Figure 3B, middle, C, D). These results indicate that inhibition of LHA^{GAD2} activity increases ARS-induced anxiety and aversive behaviors, and that selective activation of this population can mitigate stress-evoked negative affective states.

Activation of LHA^{GAD2} neurons is sufficient to reverse mechanical hypersensitivity and maladaptive behaviors

To determine whether LHA^{GAD2} neurons contribute to formalin-induced pain and behavioral dysfunction, c-Fos immunoreactivity was assessed following subcutaneous formalin injection. A significant increase in c-Fos expression within the LHA was observed at both 30 min (FM-30 min) and 2 h (FM-2 h) post-injection (Figure 3E, F). GAD2-Cre mice received intra-LHA injections of rAAV-EF1α-DIO-ChR2-mCherry or rAAV-DIO-NpHR3.0-mCherry, followed by implantation of optical fibers (Figure 3G, top). Three weeks later, formalin was administered subcutaneously, and on day 3, behavioral assessments were performed using the Von Frey and Hargreaves tests to evaluate pain sensitivity, and the OFT and EPM to assess anxiety-like behavior (Figure 3G, bottom).

In the Von Frey test, optogenetic activation of LHA^{GAD2} neurons significantly increased paw withdrawal thresholds, while inhibition decreased thresholds compared to pre-stimulation levels (Figure 3H, I). In the Hargreaves test, activation significantly prolonged paw withdrawal latency, whereas inhibition shortened it (Figure 3J). To further evaluate the contribution of LHA^{GAD2} neurons to formalin-induced nociception, chemogenetic manipulations were performed. GAD2-Cre mice received bilateral injections of rAAV-Ef1α-DIO-hM3D(Gq)-mCherry, rAAV-Ef1α-DIO-hM4D(Gi)-mCherry, or rAAV-Ef1α-DIO-mCherry into the LHA (Figure 3K). In the Von Frey test, chemogenetic activation increased withdrawal thresholds relative to saline-treated controls (Figure 3L, middle), while inhibition reduced thresholds (Figure 3L, right). In the Hargreaves test, withdrawal latency was prolonged following chemical activation (Figure 3M, middle) and reduced following inhibition (Figure 3L, right).

Behavioral assessment revealed that activation of LHA^{GAD2} neurons significantly reversed formalin-induced mechanical

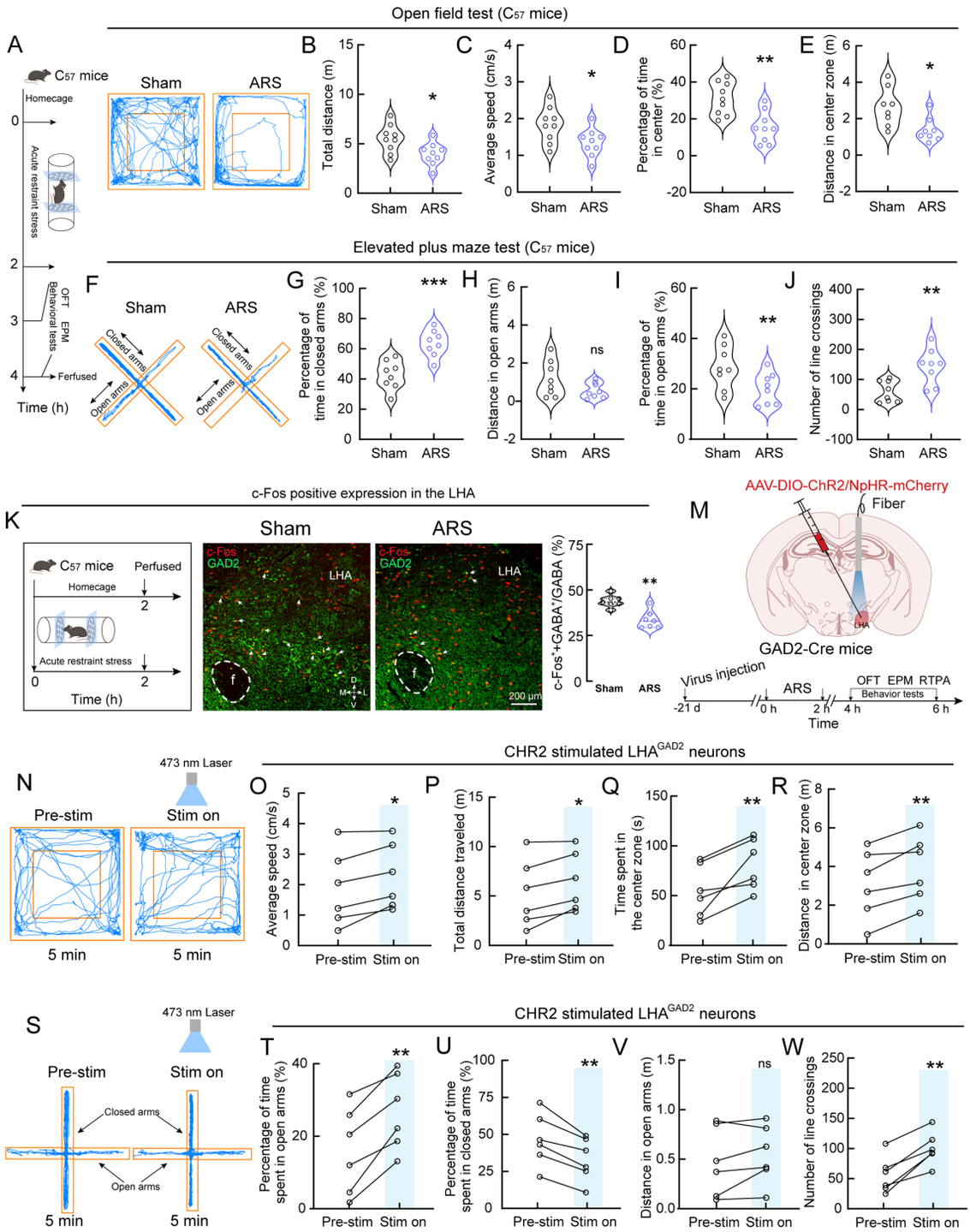

Figure 2 LHA^{GAD2} mediates acute restraint stress (ARS)-induced anxiety-like behaviors in mice

A: Schematic of experimental design for anxiety-like behavioral testing following ARS. B–E: Open field test comparing movement trajectories, total distance traveled (B), average speed (C), percentage of time spent in center zone (D), and distance traveled in center zone (E) between ARS and sham groups. Data analyzed using two-tailed unpaired *t*-test. *n*=9 mice. F–J: Elevated plus maze test comparing movement trajectories (F), percentage of time spent in closed arms (G), distance traveled in open arms (H), percentage of time spent in open arms (I), and number of line crossings (J) between ARS and sham groups. Data analyzed using two-tailed unpaired *t*-test. *n*=8 mice. K: Schematic of ARS protocol (left), representative LHA micrographs showing GABA (GAD2, green) and c-Fos (red) co-staining after 2 h of ARS or home cage condition (middle), and quantification of c-Fos-positive GABAergic neurons in the LHA between ARS and sham groups (right). Data analyzed using two-tailed paired *t*-test. *n*=7. M: Schematic of viral injection site (top) and experimental design for optogenetic manipulation combined with anxiety-like behavioral tests (bottom). N–R: Open field test showing effects of optogenetic activation or inhibition of LHA^{GABA} neurons on movement trajectory (N), average speed (O), total distance traveled (P), time spent in center zone (Q), and distance traveled in center zone (R). Data analyzed using two-tailed paired *t*-test. *n*=6 mice. S–W: Elevated plus maze test showing effects of optogenetic manipulation on movement trajectory (S), percentage of time spent in open arms (T), percentage of time spent in closed arms (U), distance traveled in open arms (V), and number of line crossings (W). Data analyzed using two-tailed paired *t*-test. *n*=6. ns: Not significant; *: *P<0.05*; **: *P<0.01*; ***: *P<0.001*. Data are presented as mean±SEM.

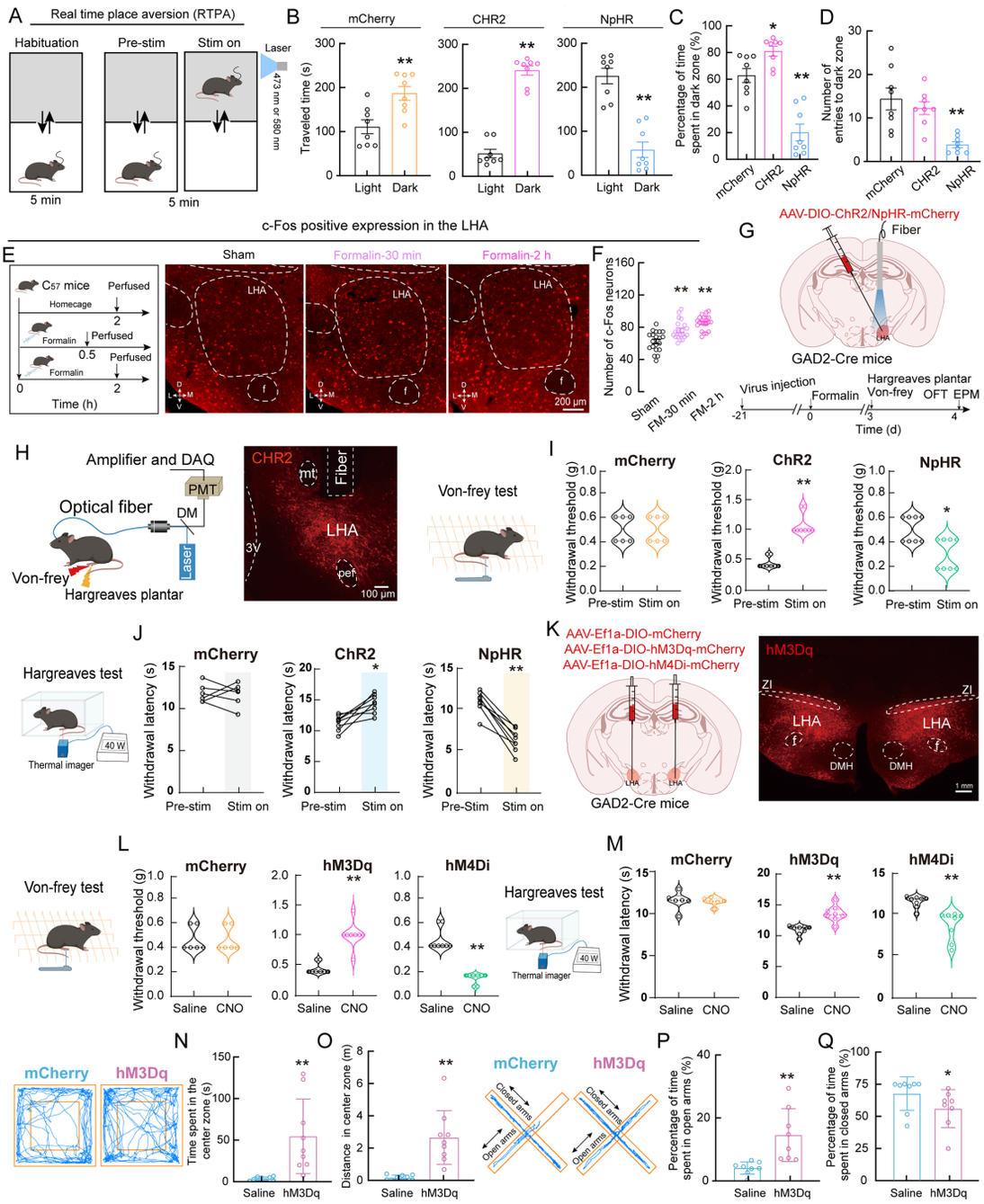

Figure 3 Activation of LHA^{GAD2} neurons mitigates formalin-induced pain-like behaviors in mice

A–D: Schematic of real-time place aversion (A) and quantification of time spent in light and dark zones (B), percentage of time spent in dark zone (C), and number of entries into dark zone (D) following optogenetic activation or inhibition of LHA^{GAD2} neurons. Data analyzed using one-way ANOVA, *n*=8. E–F: Experimental timeline for c-Fos immunofluorescence staining (left), representative LHA micrographs (right), and quantification of c-Fos-positive neurons following formalin or saline injection (F). Data analyzed using one-way ANOVA, *n*=20. G: Schematic of viral injection site (top) and experimental design for optogenetic manipulation in combination with pain- and anxiety-like behavioral testing following formalin injection (bottom). H: Schematic of optical fiber stimulation setup during behavioral assays (left) and representative micrograph showing injection site and viral expression (right). I–J: Effects of optogenetic activation or inhibition of LHA^{GAD2} neurons on paw withdrawal mechanical threshold (PWMT) (I) and paw withdrawal thermal latency (PWTL) (J) in Von Frey and Hargreaves tests. Data analyzed using two-tailed paired *t*-test. *n*=6 in mCherry group, *n*=8 in ChR2 and NpHR groups. K: Diagram showing coronal brain sections with chemogenetic injection sites (left) and representative micrograph of injection and transfection efficiency (right). L–M: Effects of chemogenetic activation or inhibition of LHA^{GABA} neurons on PWMT (L) and PWTL (M) in Von Frey and Hargreaves tests. Data analyzed using two-tailed paired *t*-test. *n*=6 in mCherry group, *n*=8 in hM3Dq and hM4Di groups. N–O: Chemogenetic activation of LHA^{GABA} neurons after subcutaneous formalin injection significantly increased time spent (N) and distance traveled (O) in center zone during the open field test compared with the saline group. Data analyzed using two-tailed paired *t*-test. *n*=9. P–Q: Chemogenetic activation of LHA^{GABA} neurons significantly increased percentage of time spent in open arms (P) and decreased percentage of time spent in closed arms (Q) during the elevated plus maze compared with the saline group. Data analyzed using two-tailed paired *t*-test. *n*=8. ns: Not significant; *: *P*<0.05; **: *P*<0.01; ***: *P*<0.001. Data are presented as mean±SEM.

and thermal hypersensitivity, whereas inhibition exacerbated nociceptive responses. In the OFT, chemogenetic activation of LHA^{GAD2} neurons led to increased time spent and distance traveled in the center zone compared to the saline-treated group (Figure 3N, O). In the EPM, neural activation increased time spent in the open arms and decreased time spent in the closed arms (Figure 3P, Q), consistent with attenuation of formalin-induced anxiety-like behavior.

Collectively, these findings demonstrate that activation of LHA^{GAD2} neurons was sufficient to reverse formalin-evoked sensory hypersensitivity and affective disturbances, while inhibition enhanced maladaptive responses.

LHA^{GAD2} projections to the vlPAG selectively modulate pain threshold without affecting affective behaviors

Previous tracing studies identified the vlPAG as a major downstream target of LHA GABAergic neurons, with functional relevance for nociception and anxiety-like behaviors. To determine whether LHA^{GAD2}-vlPAG projections mediate pain modulation in inflammatory and neuropathic contexts, both optogenetic and chemogenetic strategies were applied to selectively activate and inhibit these projections in formalin-treated and CCI mice. Initial immunofluorescence analysis revealed robust c-Fos expression in GAD2-positive neurons within the vlPAG following subcutaneous formalin injection (Figure 4A; Supplementary Figure S2A), with significantly elevated levels in both the FM-30 min and FM-2 h groups (Supplementary Figure S2B). To test the functional role of this projection, GAD2-Cre mice received intra-LHA injections of rAAV-Ef1α-DIO-hM3D(Gq)-mCherry, rAAV-Ef1α-DIO-hM4D(Gi)-mCherry, or rAAV-Ef1α-DIO-mCherry, along with bilateral cannula implantation into the vlPAG (Figure 4B). During behavioral testing, chemogenetic stimulation was combined with Von Frey or Hargreaves testing. Compared to the saline group, activation of LHA^{GAD2} terminals in the vlPAG significantly increased withdrawal thresholds and latencies, while inhibition reduced both (Figure 4C, D). Subsequently, optogenetic constructs (AAV-DIO-ChR2, NpHR-mCherry, or control AAV-DIO-mCherry) were microinjected into the LHA of GAD2-Cre mice, and optical fibers were implanted in the vlPAG (Figure 4E, F). During the Von Frey and Hargreaves tests, blue light pulses activated LHA^{GAD2}-vlPAG projections, increasing the withdrawal thresholds and latencies during optogenetic stimulation. Conversely, yellow laser pulses inhibited GABAergic terminals in the vlPAG, reducing withdrawal thresholds and latencies during optical suppression (Figure 4G, H).

To assess whether the LHA^{GAD2}-vlPAG axonal terminals modulates pain under chronic conditions, similar optogenetic manipulations were performed in GAD2-cre mice 14 days before CCI surgery. Pain sensitivity was evaluated 14 days post-surgery (Supplementary Figure S3A–C). CCI significantly lowered withdrawal thresholds and latencies (Supplementary Figure S3D, E). Optogenetic activation of LHA^{GAD2} neurons or their terminals in the vlPAG significantly reversed CCI-induced hypersensitivity during laser stimulation (Supplementary Figure S3F–I). However, activation of LHA^{GAD2}–vlPAG terminals in formalin-treated mice did not alter exploratory behavior in the OFT or EPM as no changes were observed in total distance traveled, center zone occupancy, or open-arm exploration (Supplementary Figure S2C–J). These findings suggest that this pathway does not modulate affective dimensions of formalin-evoked behaviors.

To confirm the presence of a functional monosynaptic inhibitory connection, *in vitro* patch-clamp recordings were performed in whole-brain slices. AAV-DIO-ChR2-mCherry was injected into the LHA of GAD2-Cre mice, and oIPSCs were recorded from vlPAG neurons following blue light stimulation of LHA^{GAD2} terminals. These oIPSCs were abolished by the GABAA receptor antagonist picrotoxin but were rescued by co-application of TTX and 4AP, confirming a direct monosynaptic connection between LHA^{GAD2} and vlPAG neurons (Figure 4I–L).

Overall, these optogenetic and chemogenetic experiments show that activating GABAergic neurons in the LHA suppresses pain-promoting pathways in the vlPAG, effectively dampening pain perception, whereas silencing these neurons engages those same pathways.

LHA^{GAD2} projections to the LHb selectively modulate affective aspects of pain

To delineate the circuit-specific roles of LHA^{GAD2} efferents in mediating sensory versus affective aspects of pain, projection patterns were mapped using anterograde tracing. Robust innervation from LHA^{GAD2} neurons was observed in several brain regions implicated in emotional processing, including the LHb, VTA, and dorsal raphe nucleus (DRN). To determine whether the LHb was engaged during formalin-induced pain, monosynaptic retrograde trans-synaptic tracing was performed using a RV-based labeling approach targeting LHb^{Vglut2} neurons (Figure 5A, B). Tracing combined with immunofluorescence staining confirmed that LHb-projecting LHA neurons were predominantly GAD2-positive (Figure 5C, D), establishing a direct inhibitory projection from LHA^{GAD2} to glutamatergic neurons within the LHb (LHb^{Glu}).

To assess the functional relevance of this pathway, optogenetic manipulations were used to activate LHA^{GAD2} axonal terminals in the LHb during formalin-induced behavioral assays. GAD2-Cre mice received intra-LHA injections of AAV-DIO-ChR2-mCherry or control AAV-DIO-mCherry, and optical fibers were implanted in the LHb (Figure 5E). Optogenetic stimulation was delivered during the RTPA, OFT, and EPM. During RTPA, LHA^{GAD2}-LHb terminals significantly increased time spent in the dark chamber relative to the light chamber and to the control group (Figure 5F), indicating reduced aversive response. In the OFT, activation enhanced total distance traveled and time spent in the center zone, while no significant changes were observed in the mCherry group (Figure 5G–I). In the EPM, time spent and distance traveled in the open arms were significantly increased following stimulation, with no significant changes observed in the mCherry group (Figure 5J–L). To ascertain the involvement of the LHA^{GAD2}-LHb pathway in pain-like behavior, Von Frey and Hargreaves tests were conducted in formalin-treated mice during optogenetic stimulation of the LHA^{GAD2}-LHb pathway (Figure 5M, N). Neither mechanical withdrawal thresholds nor thermal latencies were altered by stimulation in either the ChR2 or mCherry groups. These findings indicate that while LHA^{GAD2} neurons mediate different aspects of pain, only those projecting to the LHb contribute to affective and anxiety-like behaviors, contrasting with the nociceptive-specific role of LHA^{GAD2}-vlPAG projections.

To confirm that differential LHA^{GAD2} projections mediate different aspects of pain-like behaviors, upstream brain regions targeting GAD2 neurons in the LHA, as well as projection-defined LHA^{GAD2}-vlPAG and LHA^{GAD2}-LHb

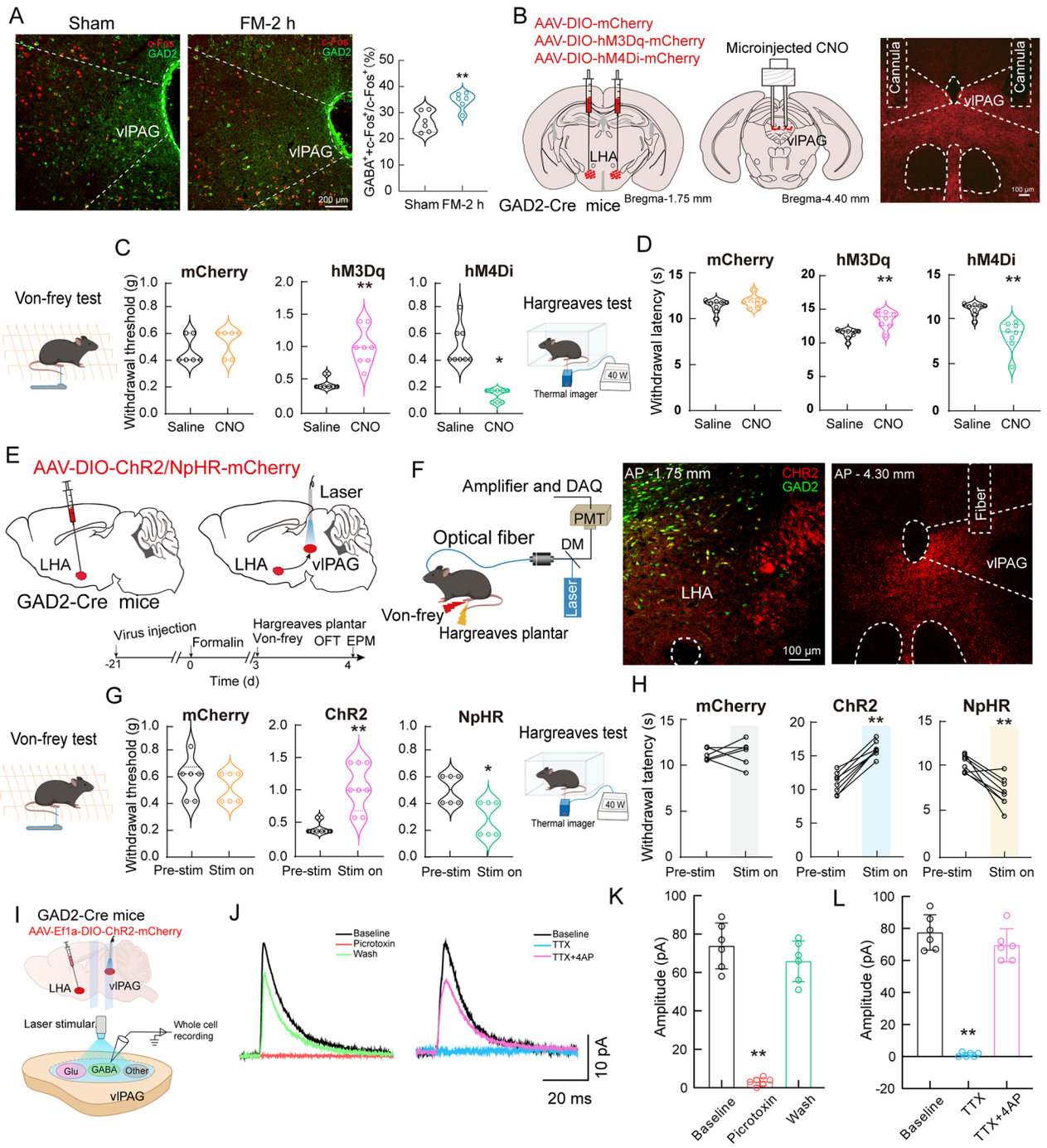

Figure 4 Activation of LHA^{GAD2}-vlPAG pathway reverses formalin-induced mechanical hypersensitivity in mice

A: Representative micrographs showing colocalization of GABA (GAD2, green) and c-Fos (red) in the vlPAG after subcutaneous injection of formalin or sham treatment (left), and quantification of GABAergic c-Fos-positive neurons among total c-Fos-positive neurons (right). Data analyzed using two-tailed paired *t*-test. *n*=6. B: Diagrams of coronal brain sections showing chemogenetic viral injection site (left) and cannula implantation site for CNO microinjection (middle), and representative micrograph showing microinjection cannula site and transfection efficiency (right). C–D: Effects of chemogenetic activation or inhibition of LHA^{GAD2} projections on paw withdrawal mechanical threshold (PWMT) (C) and paw withdrawal thermal latency (PWTL) (D) in Von Frey and Hargreaves tests. Data analyzed using two-tailed unpaired *t*-test. *n*=8. E: Schematic of optogenetic viral injection into the LHA and laser stimulation in vlPAG (top), and experimental design for optogenetic manipulation following formalin injection (bottom). F: Diagram showing injection of optogenetic viruses into the LHA and placement of optical fibers into the vlPAG of GAD2-Cre mice. Representative fluorescence images show viral expression, fiber position, and LHA^{GABA} neuron targeting (right). G–H: Effects of optogenetic activation or inhibition of LHA^{GAD2} terminals on PWMT (G) and PWTL (H) in Von Frey and Hargreaves tests. Data analyzed using two-tailed paired *t*-test. *n*=6. I–J: Representative traces and quantification of amplitudes of oIPSC recordings from vlPAG^{GABA} neurons. K–L: Quantification of oIPSC frequency in vlPAG^{GABA} neurons following optical stimulation. Data analyzed using two-tailed paired *t*-test. *n*=6. ns: Not significant; *: *P<0.05*; **: *P<0.01*; ***: *P<0.001*. Data are presented as mean±SEM.

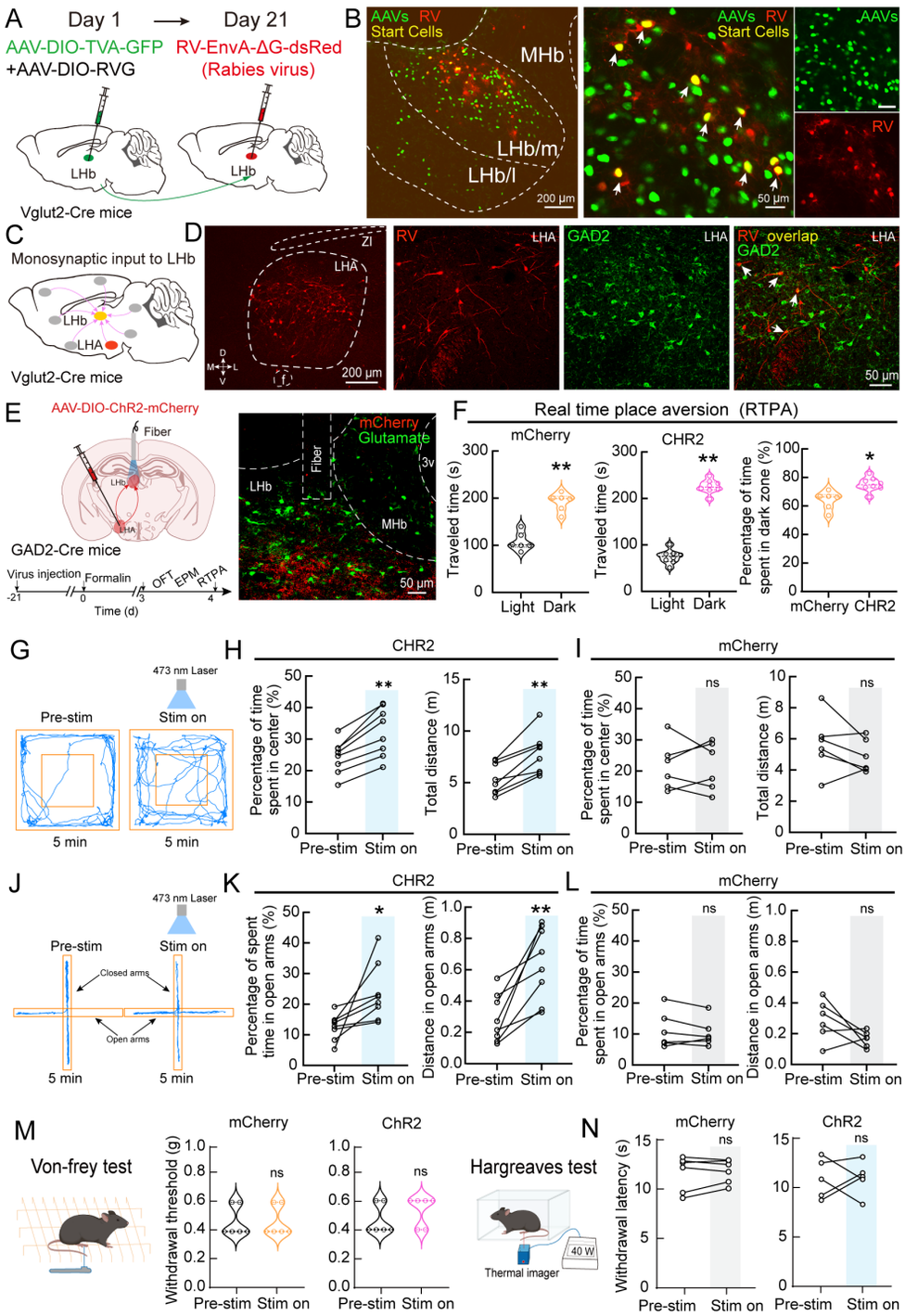

Figure 5 Optogenetic activation of LHA^{GAD2}-LHb projections alleviates avoidance behaviors but not mechanical hypersensitivity

A: Schematic of retrograde tract tracing strategy. B: Overlapping expression of AAV helper virus (green) and retrograde RV-labeled neurons (red) in the LHb of Vglut2-Cre mice. C: Visualization of monosynaptic inputs to the LHb. D: Immunolabeling of GAD2 in presynaptic RV-positive neurons within the LHA. Scale bars, 200 μm and 50 μm. E: Coronal brain maps showing optogenetic viral injection sites in the LHA and optical fiber placement in the LHb, alongside representative micrograph showing optical fiber site and transfection efficiency (right). F: Effects of optogenetic activation of LHA^{GABA} terminals in the LHb on place preference following subcutaneous formalin injection in the RTPA test showing increased time spent in the light zone and decreased time spent in the dark zone. Data analyzed using two-tailed unpaired *t*-test. *n*=8. G–I: Effects of optogenetic activation of LHA^{GABA} terminals in the LHb on open field test after formalin injection showing increased time spent in center zone (G) and total distance traveled (H). Data analyzed using two-tailed unpaired *t*-test. *n*=6. J–L: Effects of optogenetic activation of LHA^{GAD2} terminals in the LHb on anxiety-like behavior in the elevated plus maze after formalin injection showing increased time spent (J) and distance traveled (K) in open arms. M–N: Effects of optogenetic activation of LHA^{GAD2} terminals in the LHb on paw withdrawal mechanical threshold (PWMT) (M) and paw withdrawal thermal latency (PWTL) (N) in Von Frey and Hargreaves tests. Data analyzed using two-tailed paired *t*-test. *n*=6. ns: Not significant; *: *P<0.05*; **: *P<0.01*; ***: *P<0.001*. Data are presented as mean±SEM.

subpopulations, were mapped using a Cre-dependent, cell type-specific retrograde-tracing viral strategy combined with recombinant RV-based retrograde monosynaptic tracing in GAD2-Cre mice (Figure 6A). Confocal imaging demonstrated colocalization of AAV helper signals (green) with RV-positive neurons (red) in the LHA (Figure 6B). The resulting whole-brain input maps revealed broad and bilaterally symmetric afferent distributions to LHA^{GAD2} neurons and to projection-specific LHA^{GAD2}-vlPAG and LHA^{GAD2}-LHb populations.

Among the global cerebral nuclei containing monosynaptic input to the LHA^{GAD2} neurons, high densities were observed in the caudate putamen (CPu), lateral septal nucleus (LS), ventral pallidum (VP), internal capsule (ic), central amygdala nucleus lateral division (CeL), VTA, and substantia nigra reticular part (SNR) (Supplementary Figure S4A–D). Inputs to LHA^{GAD2}-vlPAG neurons were enriched in the lateral septal nucleus (LS), nucleus accumbens (NAc), lateral preoptic area (LPO), nucleus of the horizontal limb of the diagonal band (HDB), and hippocampus CA1 region (Supplementary Figure S4E–H). In contrast, LHA^{GAD2}-LHb neurons received dense inputs from the posterior hypothalamic area (PH), premammillary nucleus, dorsal part (PMD), zona incerta (ZI), and dorsal raphe nucleus (DRN) (Figure 6C; Supplementary Figure S4I–K). The findings indicate that LHA^{GAD2} neurons and their direct projections function as convergence points for a variety of direct inputs, are distributed throughout the brain, and likely convey different types of information for integration into the LHA.

Together, these findings demonstrate that LHA^{GAD2} neurons exhibit functional heterogeneity defined by their projection targets. While the LHA^{GAD2}-vlPAG pathway governs mechanical and thermal hypersensitivity, the LHA^{GAD2}-LHb pathway modulates negative affective responses to inflammatory pain, reflecting a circuit-level dissociation of sensory and emotional pain processing.

DISCUSSION

This study identified LHA^{GAD2} neurons as key modulators of both sensory hypersensitivity and negative affective states in pain contexts. Under conditions of formalin-induced inflammatory pain, LHA^{GAD2} neurons reduced c-Fos expression, indicating suppressed activity. Chemogenetic activation of these neurons markedly attenuated mechanical hypersensitivity and reduced anxiety-like behaviors in the OFT and EPM assays. Conversely, targeted Chemogenetic inhibition of the LHA^{GAD2}-vlPAG projection exacerbated mechanical allodynia under both formalin and CCI models without altering affect-related behavioral outputs. Inhibition of LHA^{GAD2} neurons also intensified nociceptive behaviors in formalin-treated mice. In contrast, activation of the LHA^{GAD2}-LHb projection via optogenetic and Chemogenetic manipulation selectively alleviated negative affective responses without affecting mechanical thresholds. These findings support a model in which distinct LHA^{GAD2} neural pathways contribute to mechanical hyperalgesia and anxiety-like behaviors following exposure to pain stimuli. The presence of non-overlapping, projection-defined LHA^{GAD2} neuron populations with diverse downstream targets underscores their critical roles in mediating the sensory and affective dimensions of pain.

Understanding the mechanisms by which pain-associated neural circuits undergo maladaptive reorganization remains a central challenge in neuroscience. Pathological pain states have been linked to disruption in intrinsic excitability and imbalances in synaptic input, particularly at the level of GABAergic and glutamatergic transmission (Shabel et al., 2014). The LHA has been implicated in mediating behavioral responses to pain (Reddy et al., 2025; Shah et al., 2025), and elevated stress levels are known to enhance pain perception and affective reactivity via modulation of hormone release in this region (Esmaeili et al., 2017; Holden et al., 2009). Despite this, the contribution of the LHA to analgesia has not been fully elucidated. Prior research has primarily emphasized excitatory projections from the LHA to pain-regulatory centers such as the lateral parabrachial nucleus and PAG (Dhaka et al., 2007; Siemian et al., 2021), although excitatory neurons constitute a minority within the LHA (Shabel et al., 2014; Shah et al., 2025). Nevertheless, the role of LHA inhibitory neurons in pain modulation has received limited attention. The present study demonstrated that inhibitory LHA^{GAD2} inputs to the vlPAG modulate pain-coping behavior in mice. This functional pathway aligns with previous evidence implicating LHA^{GAD2} neurons in arousal, reward, and stress regulation (Bonnavion et al., 2016; Stuber & Wise, 2016), all of which intersect with pain-induced behavioral outcomes (Mu et al., 2017). Chemogenetic activation of these neurons reduced RTPA and anxiety-related responses, attenuated sensory hypersensitivity, and reinstated species-typical behaviors suppressed by noxious stimuli.

As a core component of the midbrain PAG, the vlPAG is integral to the descending pain control system and modulates nociceptive transmission through endogenous opioids and other neuromodulatory systems (Siemian et al., 2021; Sullere et al., 2023). Through extensive functional connectivity with multiple brain regions, the vlPAG engages descending pathways that directly regulate spinal pain-transmitting neurons and exert powerful control over neuropathic pain states (Esmaeili et al., 2017; Holden et al., 2009). Under neuropathic conditions, the vlPAG undergoes pronounced neuroplastic remodeling (Samineni et al., 2017), and aberrant increases in neuronal activity have been reported in several pain models, potentially contributing to the persistence of chronic pain (Ho et al., 2013; Samineni et al., 2017). Beyond sensory modulation, the vlPAG maintains dense connections with emotional regulation centers, including the amygdala and prefrontal cortex, supporting a role in the management of pain-associated emotional responses such as anxiety and depression (Lee et al., 2023; Yin et al., 2020), which may exacerbate neuropathic pain and complicate therapeutic intervention. Consistent with this integrative role, the vlPAG participates in arousal, sensorimotor coordination, defensive behaviors, and pain modulation (Guo et al., 2023; Skog et al., 2024). Although GABAergic neurons in the LHA have been shown to innervate vlPAG circuitry, the specific role of LHA^{GAD2}-vlPAG projections in sensory and affective pain processing has yet to be elucidated. In the present study, optogenetic activation of LHA^{GAD2} neurons reduced thermal and mechanical nociception in an inflammatory pain model. These effects were attributable to engagement of the LHA^{GAD2}-vlPAG pathway, as selective activation of this projection increased mechanical thresholds and thermal withdrawal latencies in both inflammatory and neuropathic pain paradigms. Notably, modulation of this pathway did not alter anxiety-like or aversive behaviors, indicating a preferential role in sensory pain control rather than affective regulation.

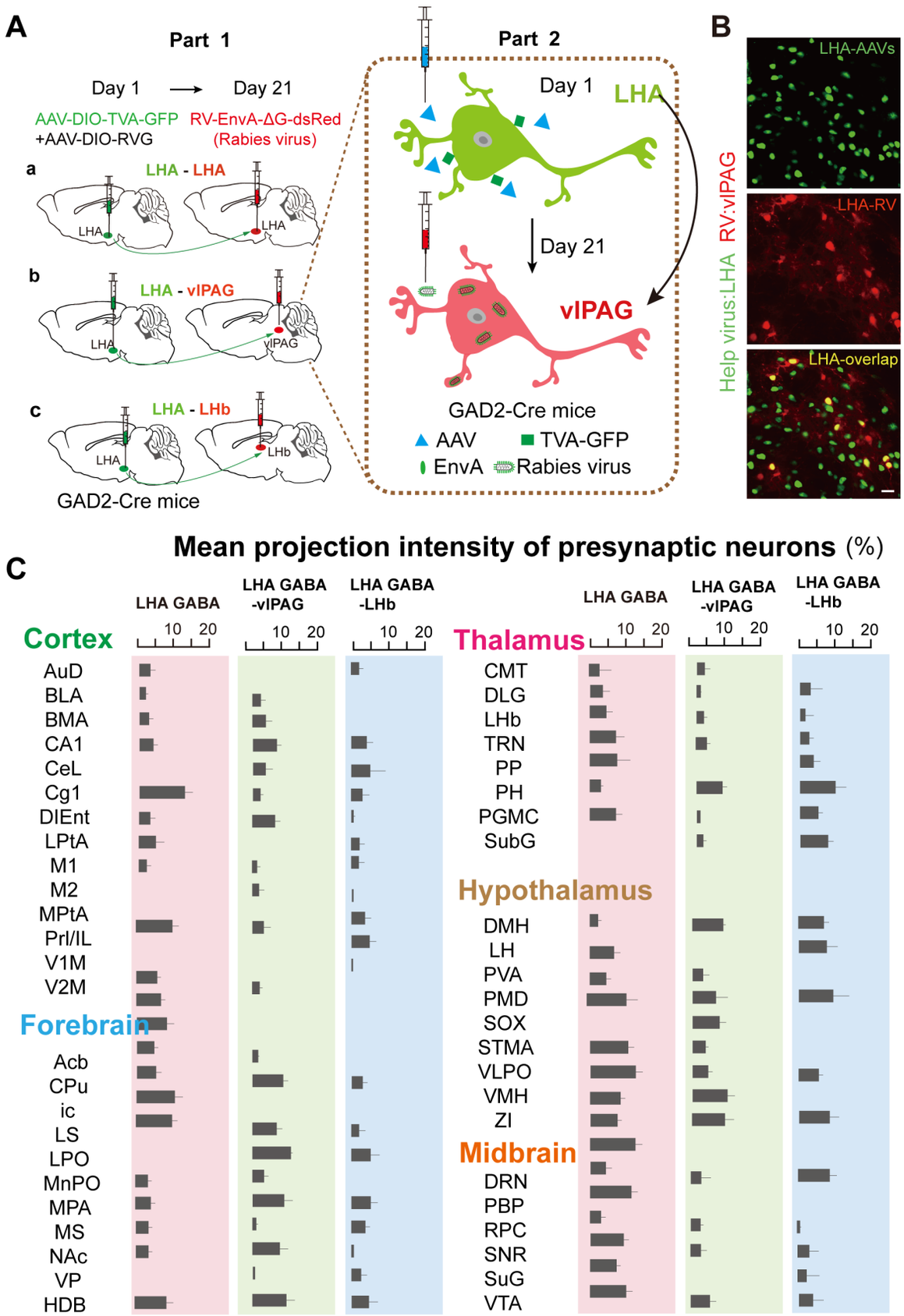

Figure 6 Strategy for genetically specified tracing of monosynaptic inputs to LHA^{GAD2} neurons

A: Schematic illustrating retrograde monosynaptic tracing strategy used to map presynaptic inputs to LHA^{GAD2} neurons and projection-defined subpopulations. B: Representative fluorescence images showing overlap of AAV helper virus (green) and RV-labeled presynaptic neurons (red) in the vlPAG of GAD2-Cre mice. C: Quantification of projection intensity from presynaptic brain regions to LHA^{GABA}, LHA^{GABA}-vlPAG, and LHA^{GABA}-LHb neurons. Data analyzed using a chi-square test to compare cell counts across groups.

The LHb receives dense anterograde projections from GABAergic neurons in the LHA, as previously characterized (Wang et al., 2024). As a key inhibitory regulator of monoaminergic nuclei, the LHb has been implicated in encoding negative valence and orchestrating aversive behavioral states (Hu et al., 2020; Matsumoto & Hikosaka, 2007). LHb^{Glu} neurons are rapidly activated in response to aversive stimuli (Cui et al., 2022; Zheng et al., 2022) and exhibit sustained hyperactivity in chronic stress or pain models, paralleling depression-like phenotypes. In contrast, ablation or inhibition of LHb activity ameliorates such behaviors in rodents (Yang et al., 2018; Zheng et al., 2022). Furthermore, modulation of upstream afferents to the LHb, including those from the LHA, medial prefrontal cortex, and VP, has been found to bidirectionally influence depressive-like behaviors (Huang et al., 2019; Lin et al., 2022; Zheng et al., 2022). In the present study, whether LHA^{GAD2} neurons modulate nociceptive processing via projections to the LHb was examined. First, synaptic connectivity from LHA^{GAD2} neurons to LHb^{Glu} neurons was confirmed, enabling functional interrogation of this projection in pain-related contexts. Optogenetic activation of the LHA^{GAD2}-LHb circuit in mice subjected to the formalin-induced pain did not alter nociceptive responses to noxious thermal or mechanical stimuli. However, stimulation of this pathway significantly increased time spent on the photostimulation-paired side in RTPA assays, indicating an anti-aversive effect mediated by LHA^{GAD2} projections to the LHb, which regulate aversion, as previously shown for the broader LHA glutamatergic population (Stamatakis et al., 2016), but not nociception. The findings indicate that distinct outputs from LHA^{GAD2} neurons are linked to various dimensions of pain-like behavior. Specifically, neurons projecting to the vlPAG are implicated in the sensory dimension of pain, whereas those innervating the LHb are associated with the affective dimension. Although the present study focused on LHA-specific projections, convergent projections from adjacent hypothalamic nuclei, including the PVN and DMH, may also participate in nociceptive modulation (Bassi et al., 2018; de Menezes et al., 2009; Shen et al., 2025). Future studies employing higher-resolution and cell-type-specific approaches, such as targeted fiber photometry, will be required to resolve these overlapping hypothalamic circuits.

Collectively, our findings suggest that the LHA functions as a critical hub for modulating both sensory and affective dimensions of pain. The identified LHA-vlPAG/LHb circuit constitutes a key GABAergic projection involved in pain regulation. Given the substantial public health burden posed by chronic pain and the limitations of current therapeutics, elucidating central mechanisms underlying pain persistence is imperative. Central sensitization contributes to the maintenance of chronic pain, and the present results indicate that the LHA may represent a viable target for pain intervention. Specifically, distinct LHA^{GAD2}-positive neuronal populations, characterized by their divergent projections, mediate both pain-induced aversion and mechanical hypersensitivity. Understanding the function and organization of these projection-defined ensembles could facilitate the development of more precise pain management therapies. The present study delineated the neural substrates underlying pain responses, offering mechanistic insight into the emergence of pain-like and anxiety-like behaviors following surgical trauma and providing a foundation for precise postoperative pain management. This work focused on the role of LHA^{GAD2} neurons in pain regulation, using formalin-induced pain models to dissect circuit-level mechanisms. However, whether GABAergic hypothalamic modulation of pain extends to molecular mechanisms remains unresolved.

Despite the significance of our findings, this study has several limitations. The Cre-LoxP approach used to label GAD2-expressing neurons lacks temporal specificity, limiting its ability to selectively target pain-activated neuronal populations. Techniques such as TRAP2 (targeted recombination in active populations) (DeNardo et al., 2019) and CANE (capturing activated neuronal ensembles) (Sakurai et al., 2016) may offer greater precision for isolating nociceptive LHA^{GAD2} neurons. Although distinct LHA^{GAD2} populations were shown to regulate either affective or sensory components of pain, specific molecular markers that differentiate these subpopulations remain unidentified. Furthermore, while activation of the LHA^{GAD2} and LHA^{GAD2}-vlPAG pathways was sufficient to induce mechanical hypersensitivity, the transient nature of the inhibition suggests a more complex underlying mechanism, potentially involving neuroplasticity within the LHA^{GAD2}-vlPAG circuitry or other brain regions. Furthermore, this study was limited to male GAD2-Cre mice. As previous work has demonstrated sex-specific differences in analgesic responses, further research is needed to assess whether these findings generalize to females. The vlPAG is a sexually dimorphic region containing ERα-expressing neurons with species-specific distribution patterns, which may contribute to differential pain modulation. Future studies incorporating both sexes and utilizing temporally resolved targeting strategies are required to comprehensively define the role of LHA GABAergic circuits in pain regulation.

SUPPLEMENTARY DATA

Supplementary data to this article can be found online.

COMPETING INTERESTS

The authors declare that they have no competing interests.

AUTHORS' CONTRIBUTIONS

H.L.D. and D.W. initiated and directed the study; H.M.L. and D.W. revised the manuscript. D.W. and Z.X.W. wrote the manuscript draft. H.M.L., H.M.W., C.B., J.S.Z., B.Q.L., J.N.L., T.T.G. and M.K.G. performed the experiments; D.W., Z.X.W., and J.S.Z. analyzed the data. All authors read and approved the final version of the manuscript.

ACKNOWLEDGMENTS

We thank Sa Wang and Ya-Ru Guo for the genetic mouse line generation. We thank all members of the Department of Anesthesiology, Xijing Hospital, for their assistance.

REFERENCES

Baliki MN, Apkarian AV. 2015. Nociception, pain, negative moods, and behavior selection. *Neuron*, **87**(3): 474–491.

Bassi GS, Kanashiro A, Rodrigues GJ, et al. 2018. Brain stimulation differentially modulates nociception and inflammation in aversive and non-aversive behavioral conditions. *Neuroscience*, **383**: 191–204.

Bonnavion P, Mickelsen LE, Fujita A, et al. 2016. Hubs and spokes of the lateral hypothalamus: cell types, circuits and behaviour. *The Journal of Physiology*, **594**(22): 6443–6462.

Bushnell MC, Čeko M, Low LA. 2013. Cognitive and emotional control of pain and its disruption in chronic pain. *Nature Reviews Neuroscience*, **14**(7): 502–511.

Corder G, Ahanonu B, Grewe BF, et al. 2019. An amygdalar neural ensemble that encodes the unpleasantness of pain. *Science*, **363**(6424): 276–281.

Cui YT, Huang XD, Huang PC, et al. 2022. Reward ameliorates depressive-like behaviors via inhibition of the substantia innominata to the lateral habenula projection. *Science Advances*, **8**(27): eabn0193.

de Menezes RCA, Zaretsky DV, Fontes MAP, et al. 2009. Cardiovascular and thermal responses evoked from the periaqueductal grey require neuronal activity in the hypothalamus. *The Journal of Physiology*, **587**(6): 1201–1215.

DeNardo LA, Liu CD, Allen WE, et al. 2019. Temporal evolution of cortical ensembles promoting remote memory retrieval. *Nature Neuroscience*, **22**(3): 460–469.

Dhaka A, Murray AN, Mathur J, et al. 2007. TRPM8 is required for cold sensation in mice. *Neuron*, **54**(3): 371–378.

Esmaeili MH, Reisi Z, Ezzatpanah S, et al. 2017. Role of orexin-2 and CB1 receptors within the periaqueductal gray matter in lateral hypothalamic-induced antinociception in rats. *Behavioural Pharmacology*, **28**(1): 83–89.

Gan Z, Gangadharan V, Liu S, et al. 2022. Layer-specific pain relief pathways originating from primary motor cortex. *Science*, **378**(6626): 1336–1343.

Guo YX, Song YP, Cao FY, et al. 2023. Ventrolateral periaqueductal gray GABAergic neurons promote arousal of sevoflurane anesthesia through cortico-midbrain circuit. *iScience*, **26**(9): 107486.

Hargreaves K, Dubner R, Brown F, et al. 1988. A new and sensitive method for measuring thermal nociception in cutaneous hyperalgesia. *Pain*, **32**(1): 77–88.

He XM, Ji PF, Guo RX, et al. 2023. Regulation of the central amygdala on intestinal motility and behavior via the lateral hypothalamus in irritable bowel syndrome model mice. *Neurogastroenterology & Motility*, **35**(2): e14498.

Ho YC, Cheng JK, Chiou LC. 2013. Hypofunction of glutamatergic neurotransmission in the periaqueductal gray contributes to nerve-injury-induced neuropathic pain. *Journal of Neuroscience*, **33**(18): 7825–7836.

Holden JE, Pizzi JA, Jeong Y. 2009. An NK1 receptor antagonist microinjected into the periaqueductal gray blocks lateral hypothalamic-induced antinociception in rats. *Neuroscience Letters*, **453**(2): 115–119.

Hu HL, Cui YH, Yang Y. 2020. Circuits and functions of the lateral habenula in health and in disease. *Nature Reviews Neuroscience*, **21**(5): 277–295.

Huang L, Xi Y, Peng YF, et al. 2019. A visual circuit related to habenula underlies the antidepressive effects of light therapy. *Neuron*, **102**(1): 128–142. e8.

Lee MT, Peng WH, Wu CC, et al. 2023. Impaired ventrolateral periaqueductal gray-ventral tegmental area pathway contributes to chronic pain-induced depression-like behavior in mice. *Molecular Neurobiology*, **60**(10): 5708–5724.

Li HM, Wang S, Wang D, et al. 2025. Dopamine drives feedforward inhibition to orexin feeding system, mediating weight loss induced by morphine addiction. *Advanced Science*, **12**(10): 2411858.

Li XY, Zhang SY, Hong YZ, et al. 2024. TGR5-mediated lateral hypothalamus-dCA3-dorsolateral septum circuit regulates depressive-like behavior in male mice. *Neuron*, **112**(11): 1795–1814. e10.

Lin S, Huang L, Luo ZC, et al. 2022. The ATP level in the medial prefrontal cortex regulates depressive-like behavior via the medial prefrontal cortex-lateral habenula pathway. *Biological Psychiatry*, **92**(3): 179–192.

Matsumoto M, Hikosaka O. 2007. Lateral habenula as a source of negative reward signals in dopamine neurons. *Nature*, **447**(7148): 1111–1115.

Mindaye SA, Chen WS, Lin SC, et al. 2024. Separate anterior paraventricular thalamus projections differentially regulate sensory and affective aspects of pain. *Cell Reports*, **43**(11): 114946.

Mu D, Deng J, Liu KF, et al. 2017. A central neural circuit for itch sensation. *Science*, **357**(6352): 695–699.

Navratilova E, Porreca F. 2014. Reward and motivation in pain and pain relief. *Nature Neuroscience*, **17**(10): 1304–1312.

Price DD. 2000. Psychological and neural mechanisms of the affective dimension of pain. *Science*, **288**(5472): 1769–1772.

Reddy P, Narayan Prajapati J, Chaterji S, et al. 2025. Converging inputs compete at the lateral parabrachial nuclei to dictate the affective-motivational responses to cold pain. *Pain*, **166**(5): 1105–1117.

Sakurai K, Zhao SL, Takatoh J, et al. 2016. Capturing and manipulating activated neuronal ensembles with CANE delineates a hypothalamic social-fear circuit. *Neuron*, **92**(4): 739–753.

Samineni VK, Premkumar LS, Faingold CL. 2017. Neuropathic pain-induced enhancement of spontaneous and pain-evoked neuronal activity in the periaqueductal gray that is attenuated by gabapentin. *Pain*, **158**(7): 1241–1253.

Shabel SJ, Proulx CD, Piriz J, et al. 2014. Mood regulation. GABA/glutamate co-release controls habenula output and is modified by antidepressant treatment. *Science*, **345**(6203): 1494–1498.

Shah DP, Sharma PR, Agarwal R, et al. 2025. A septo-hypothalamic-medullary circuit directs stress-induced analgesia. *Elife*, **13**: RP96724.

Shen ZQ, Chang WQ, Liang LF, et al. 2025. Electroacupuncture effects on trigeminal neuralgia with comorbid anxiety and depression: the role of frequency and acupoint specificity. *FASEB Journal*, **39**(2): e70337.

Siemian JN, Arenivar MA, Sarsfield S, et al. 2021. An excitatory lateral hypothalamic circuit orchestrating pain behaviors in mice. *Elife*, **10**: e66446.

Skog TD, Johnson SB, Hinz DC, et al. 2024. A prefrontal→periaqueductal gray pathway differentially engages autonomic, hormonal, and behavioral features of the stress-coping response. *Journal of Neuroscience*, **44**(46): e0844242024.

Stamatakis AM, van Swieten M, Basiri ML, et al. 2016. Lateral hypothalamic area glutamatergic neurons and their projections to the lateral habenula regulate feeding and reward. *Journal of Neuroscience*, **36**(2): 302–311.

Stuber GD, Wise RA. 2016. Lateral hypothalamic circuits for feeding and reward. *Nature Neuroscience*, **19**(2): 198–205.

Sullere S, Kunczt A, McGehee DS. 2023. A cholinergic circuit that relieves pain despite opioid tolerance. *Neuron*, **111**(21): 3414–3434. e15.

Tang HD, Dong WY, Hu R, et al. 2022. A neural circuit for the suppression of feeding under persistent pain. *Nature Metabolism*, **4**(12): 1746–1755.

Wang D, Bao C, Wu HM, et al. 2024. A hypothalamus-lateral periaqueductal gray GABAergic neural projection facilitates arousal following sevoflurane anesthesia in mice. *CNS Neuroscience & Therapeutics*, **30**(9): e70047.

Wang D, Li A, Dong KY, et al. 2021. Lateral hypothalamus orexinergic inputs to lateral habenula modulate maladaptation after social defeat stress. *Neurobiology of Stress*, **14**: 100298.

Wu YY, Yao XM, Jiang YL, et al. 2017. Pain aversion and anxiety-like behavior occur at different times during the course of chronic inflammatory pain in rats. *Journal of Pain Research*, **10**: 2585–2593.

Yang Y, Cui YH, Sang KN, et al. 2018. Ketamine blocks bursting in the lateral habenula to rapidly relieve depression. *Nature*, **554**(7692): 317–322.

Yin JB, Liang SH, Li F, et al. 2020. dmPFC-vlPAG projection neurons contribute to pain threshold maintenance and antianxiety behaviors. *The Journal of Clinical Investigation*, **130**(12): 6555–6570.

Zhang X, Liu P, He XL, et al. 2021. The PKCγ neurons in anterior cingulate cortex contribute to the development of neuropathic allodynia and pain-related emotion. *Molecular Pain*, **17**: 17448069211061973.

Zheng ZW, Guo C, Li M, et al. 2022. Hypothalamus-habenula potentiation encodes chronic stress experience and drives depression onset. *Neuron*, **110**(8): 1400–1415. e6.

Zhu C, Yao Y, Xiong Y, et al. 2017. Somatostatin neurons in the basal forebrain promote high-calorie food intake. *Cell Reports*, **20**(1): 112–123.